

Distribution Agreement

In presenting this thesis or dissertation as a partial fulfillment of the requirements for an advanced degree from Emory University, I hereby grant to Emory University and its agents the non-exclusive license to archive, make accessible, and display my thesis or dissertation in whole or in part in all forms of media, now or hereafter known, including display on the world wide web. I understand that I may select some access restrictions as part of the online submission of this thesis or dissertation. I retain all ownership rights to the copyright of the thesis or dissertation. I also retain the right to use in future works (such as articles or books) all or part of this thesis or dissertation.

Signature:

Daniel Semiaticki

Date

**Spectroscopic Study of Kinetic Processes Occurring upon Photoexcitation of Alkali
Metal Vapors Mixed with Rare Gases**

By

Daniel Semiaticki
Master of Science

Chemistry

Dr. Michael Heaven
Advisor

Dr. Francesco Evangelista
Committee Member

Dr. Susanna Widicus Weaver
Committee Member

Accepted:

Lisa A. Tedesco, Ph.D.
Dean of the James T. Laney School of Graduate Studies

Date

Spectroscopic Study of Kinetic Processes Occurring upon
Photoexcitation of Alkali Metal Vapors Mixed with Rare Gases

By

Daniel Semiaticki

B.S., North Dakota State University, 2012

Advisor: Michael Heaven, Ph.D.

An abstract of
a thesis submitted to the Faculty of the
James T. Laney School of Graduate Studies of Emory University
in partial fulfillment of the requirements for the degree of
Master of Science
in Chemistry
2014

Abstract

Spectroscopic Study of Kinetic Processes Occurring upon Photoexcitation of Alkali Metal Vapors Mixed with Rare Gases

By Daniel Semiaticki

Over the last decade, lasers with high beam quality and high beam power have been of interest for military purposes as a defensive weapon, as well as for some commercial purposes. The use of alkali metal vapors for such lasers in the form of excimer pumped and diode pumped alkali lasers, XPAL and DPAL respectively, has been considered and studied by numerous investigators. When these lasers are scaled to high powers, release of the pumping energy through undesirable processes will also scale with the power used. Thus, it is important to understand the kinetics of these processes in order to minimize their effects and increase the laser performance. In an effort to study some of these energy decay pathways likely to be present in XPAL and DPAL, an apparatus to perform gas phase spectroscopy was assembled in the Heaven laboratory. The system was tested by checking for the presence, spacing and relative intensity of the D lines of sodium vapor in vacuum. Because Rb is of prime interest in alkali metal lasers, the dependence of the emission of fluorescence at 422nm from gaseous Rb upon excitation at 780nm, previously observed, was studied in order to determine the process giving rise to this 422nm fluorescence. The kinetic model presented in this report suggests that this process involves the ionization of the metal when it is irradiated with the pump pulse, thus forming Rb^+ , which is then consumed through a collisional process with the buffer gas and the neutral metal to form Rb_2^+ . Dissociative recombination of Rb_2^+ produces an Rb atom in an excited state which then emits 422nm radiation when returning to its ground state. To estimate the metal density, this study uses a radiation trapping model that correlates the lifetime of the 780nm fluorescence signal, which Rb emits after being excited at 780 nm, to the metal vapor density. Current results suggest that the set-up is adequate to study alkali metal properties related to their photoexcitation in rare gases, which in turn will provide details on the non-lasing processes in diode and excimer pumped alkali metal lasers.

Spectroscopic Study of Kinetic Processes Occurring upon
Photoexcitation of Alkali Metal Vapors Mixed with Rare Gases
By

Daniel Semiaticki
B.S., North Dakota State University, 2012

Advisor: Michael Heaven, Ph.D.

A thesis submitted to the Faculty of the
James T. Laney School of Graduate Studies of Emory University
in partial fulfillment of the requirements for the degree of
Master of Science
in Chemistry
2014

Table of Contents

1	Introduction	1
1.1	Interest in alkali metal lasers	1
1.2	Lasing scheme	2
1.3	Collision pairs to pump alkali lasers.....	5
1.4	Multiphoton excitation	10
2	Experimental Details	13
2.1	Vaporization of the metal	13
2.2	Laser induced fluorescence	13
3	Discussion and Results	16
3.1	Sodium	16
3.1.1	Preliminary testing of the system	16
3.1.2	Fluorescence decay time	17
3.1.3	Variation of the buffer gas pressure spanning 40-100 Torr.....	19
3.2	Rubidium.....	22
3.2.1	Determination of the metal vapor density	22
3.2.2	Fluorescence at 422 nm from Rb when pumped on its D ₂ transition.....	27
4	Conclusion.....	36
	References	37

List of Figures

Figure 1: Alkali metal lasing scheme	3
Figure 2: Potential energy curves of Rb-Ar pairs	6
Figure 3: Blue spectral satellite of Cs vapor mixed with rare gases	7
Figure 4: Excitation spectrum of Cs in its blue satellite region.....	8
Figure 5: Experimental set-up.....	15
Figure 6: Laser induced fluorescence spectrum of Na	16
Figure 7: Time based signal of Na fluorescence excited and detected at 589 nm	17
Figure 8: Decay curve of the 780nm fluorescence from Rb.....	25
Figure 9: Multiphoton ionization of Rb scheme	28
Figure 10: Sample time based signal of radiation of 422 nm when exciting Rb at 780 nm....	32
Figure 11: Dependence of the 422nm fluorescence from Rb on the buffer gas pressure.....	34

List of Tables

Table 1: Lifetime of laser induced fluorescence of Na vapor at 589 nm	18
Table 2: Population density and fluorescence lifetime of Na at 589 nm in Ar and He.....	21
Table 3: Settings tested for the detection of 422 nm fluorescence from Rb	32

1 Introduction

1.1 Interest in alkali metal lasers

Since the discovery of lasers 1960, laser technology has expanded, their applications are now many and span multiple fields. For example, in the medical field lasers are used for skin treatment¹ and vision correction². Lasers have many commercial applications such as sensors³ and data transmission through optical fibers⁴. With the advance in their technology, the design of high power lasers has allowed applications in lithography⁵ and lasers capable of producing beams of a high power and of a high quality have been receiving significant attention over the past decade⁶. The high beam quality of this new class of lasers combined with a high power has numerous applications including military weapons⁷ to destroy missiles and rockets in mid-air^{8,9}, underwater communication, powering satellites and other equipment in space¹⁰. Alkali metal lasers pumped by diode lasers are excellent candidates for this type applications. The high beam quality of these lasers implies that in the absence in the laser beam path of particles susceptible to absorb the radiation emitted by the laser, the laser beam will lose little power as it travels through its propagation medium. Among the alkali metals, Rb and Cs have gained more interest due to the good transmission of their D₂ lines through the atmosphere¹¹. This necessitates the excitation of the metal atoms to excited states, the efficiency of relatively inexpensive diode lasers in the region that match the excitation wavelength of the alkali metal makes diode lasers a convenient source for the excitation of the alkali metal⁶. Previous research for high power and high beam quality lasers included Chemical Oxygen Iodine Lasers (COIL)¹², such lasers were successfully designed, but, the need of a chemical reaction involving explosive reactants, such as hydrogen peroxide to drive them presented a safety hazard⁹ and new systems were considered. XPAL and DPAL

are driven electrically, an advantage over COIL, since the safety risks linked with the gases used to operate COIL are removed; moreover, because the lasing medium is gaseous, the laser output is not subject to crystal imperfections present in solid state lasers. Thus, DPAL and XPAL incorporate the benefit of a system alimented electrically and the beam quality of a gas laser¹³. These alkali metal lasers include Diode Pumped Alkali Lasers (DPAL) and Excimer Pumped Alkali Lasers (XPAL)⁶, in the latter, the excited alkali metal atom is produced upon dissociation of an excimer pumped by the diode laser. Such systems have been reported with quantum efficiencies greater than 98%¹⁴ and slope efficiency up to 82% for Rb⁶. Diode lasers are not easily tunable⁶, therefore, efforts to refine the overlap between the emission spectrum of the diode laser with the one of the absorption spectrum of the alkali metal have focused on adjusting the absorption profile of the alkali metal. Krupke⁶, Readle¹⁵, Pitz et al.¹⁶, among others, have studied improving the efficiency of DPAL and XPAL by better matching the spectrum of the excitation source with the absorption profile of the alkali metal. This is a critical step in improving their efficiency, however, energy losses still occur outside of the mismatch between the spectral profile of the diode laser and the one of the metal. These energy losses can be from “multiphoton absorption, ionization of the metal, heating or chemical reactions”¹⁷. All these effects must be minimized to improve the efficiency of these lasers.

1.2 Lasing scheme

The lasing process of interest in alkali metal lasers is the following: in their ground electronic state, alkali metal atoms possess a single valence electron, in an s orbital, resulting in a $^2S_{1/2}$ ground state. The lowest energy excited states result from promotion of the ns^1 electron to a np orbital resulting in two levels, $^2P_{1/2}$ and $^2P_{3/2}$, due to spin orbit splitting. For an alkali metal with a valence electron in the ground state shell n, the electronic transition from the $n^2S_{1/2}$ to

the $n^2P_{1/2}$ state corresponds to the D_1 line and the transition from the $n^2S_{1/2}$ to the $n^2P_{3/2}$ state corresponds to the D_2 line; together they form the D lines. A laser scheme has been proposed involving the three electronic states mentioned, shown schematically in Figure 1.

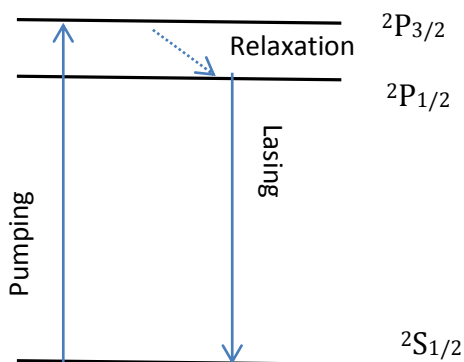


Figure 1: Alkali metal lasing scheme; the pumping is achieved using a diode laser. He induces the spin-orbit relaxation and lasing occurs when the electron relaxes from the $^2P_{1/2}$ to the $^2S_{1/2}$ state.

In this scheme, the valence electron is promoted from the $^2S_{1/2}$ to the $^2P_{3/2}$ state through photoexcitation. The electron then relaxes to the lower, $^2P_{1/2}$ state, through collisional relaxation, resulting in a population inversion between the $^2S_{1/2}$ and the $^2P_{1/2}$ state. A key step in the lasing of alkali metal lasers is the relaxation of the metal to a lower spin state. Inducement of the spin orbit relaxation between the P states is usually done by collision with He¹⁸. Spin orbit relaxation has also been demonstrated by Perram et al.¹⁹ using small alkane molecules with greater efficiency, but, these molecules react with the alkali metals to form solid deposits, thereby fogging the windows of the gain chamber and rendering their use inconvenient^{20,21}. He, which is an inert gas is not susceptible to react with the alkali metal and is now being considered as a spin orbit relaxant^{22,23}. The gain medium would then consist of the alkali metal, and a mixture of rare gases, such as Ar to pressure broaden the spectral profile of the alkali metal or forms excimers with the alkali metal, and He for the spin orbit relaxation.

The ways the pumping energy is consumed in non-lasing processes in the alkali metal/rare gas vapor gain cell must be characterized in order to improve the efficiencies of these lasers. The rate constants associated with these interactions will ultimately have to be calculated to adequately optimize the lasers¹⁷, but, before such steps are taken, the nature and kinetics of non-lasing processes at play once the alkali metal is irradiated must be identified. The work presented here provides preliminary information in the characterization and buffer gas pressure dependence of these processes through the spectroscopic study of Rb vapor in a rare gas. This in turn, may lead to a more efficient scaling of alkali metal lasers to high powers in the goal of producing high power and high beam quality lasers

Aside from the lasing scheme of these lasers illustrated in figure 1, the energy used to pump electrons to the excited states is also susceptible to be released via decay pathways other than the one leading to lasing. A decay pathway in this context would be processes that result in depopulation of the A^2P_1 levels of the alkali metal. Of interest in this report is the multiphoton absorption of the pumping energy. This multiphoton absorption would depopulate the $A^2P_{3/2}$ state in favor of higher lying states. This would occur by the absorption of one or more photons by the metal excited to the $A^2P_{3/2}$ state. Thus, the pumping energy would be used in another way than the one suggested in the lasing scheme shown in figure 1. With the high powers used in alkali metal lasers, it is conceivable that such multiphoton absorption processes would occur. To maximize the efficiency of these lasers and possibly prolong their longevity, detailed knowledge of these alternative decay pathways is necessary to develop methods to minimize the chances of energy being released through them, thus decreasing the energy lost through electronic pathways not leading to lasing. Detection of photonic energy outside the lasing region of interest is indicative of energy being released through alternative decay pathway processes. In the case of multiphoton absorption, the energy released once the metal returns to its ground state will be greater than the lasing energy. Previously in the

Heaven lab, the presence of a signal at 422nm from a Rb/RG cell pumped at 780nm was observed and initial explanations were based on an energy pooling model, in which two singly excited atoms would collide to form a ground state atom and a doubly excited atom, however, it could also be due a multiphoton absorption process. Since energy pooling is independent of the pressure of the buffer gas, variations of the buffer gas pressure could be used to either rule out the process or support it. The metal source used in the previous experiments in the Heaven lab was a sealed cell which contained a mixture of alkali metal and a buffer gas. Consequently, the pressure of the buffer gas could not be achieved without the purchase of another cell, the expense and timing inconvenience linked with such a purchase restricted further experiments. The set-up used in the present experiments uses a flowing cell in which the pressure of the buffer gas could easily be adjusted by regulating its flow, thus the effects on the 422nm of the buffer gas pressure could be tested more conveniently. This report offers a description of the processes associated with the emission of the 422nm radiation when Rb is excited on its D_2 transition in a buffer medium. Thus, it explains a process in which the pumping energy used in alkali metal lasers is susceptible to be dissipated without lasing.

1.3 Collision pairs to pump alkali lasers

To increase the efficiency of alkali metal lasers, previous studies performed by Readle in the Eden group¹⁵ have shown that a potential way to configure the lasing medium would be to have a mixture of spin orbit relaxant gas, in these cases He, to transfer the electron to the lower spin-orbit coupling state, and of another rare gas (RG), Ar for the scheme shown in figure 2, or a mixture thereof, capable of increasing the efficiency of the absorption process through creating absorption satellites in the vicinity of the D_2 line. The absorption satellites

result from collision pairs between the buffer gas and the alkali metal and they increase the efficiency of the system by absorbing more of the energy released by the diode lasers. These systems are known as Excimer Pumped Alkali Lasers (XPAL) because they use the collision pair of the alkali metal and the RG atoms to populate the excited state orbitals of the metal.

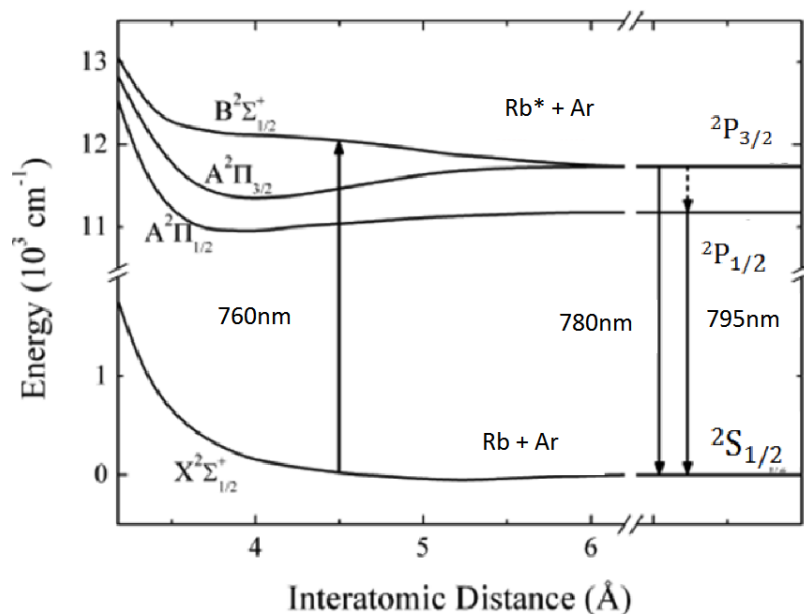


Figure 2: Potential energy curves of Rb-Ar Pairs, the 760nm radiation is used to excite the Rb in the satellite region of the pair, the Rb-Ar pair in its B state being repulsive, it dissociates forming a Rb atom in its $^2P_{3/2}$ state which is then quenched to the lower spin orbit state, $^2P_{1/2}$, with a collisional relaxant, He or some hydrocarbon. Lasing occurs upon relaxation of the electron from the $^2P_{1/2}$ to the $^2S_{1/2}$ state. Diagram adapted from reference 15.

The absorption wavelength of the collision pairs between an alkali metal and a buffer gas atom correspond to a region on the potential energy surface where the interatomic distances between the atoms would be about 4.5\AA , and due to differing interaction potentials, these satellite features are affected by the type of buffer gas used. Typical bandwidths of diode lasers are approximately 2 nm, significantly broader than the ones of atomic transitions. The satellite bands however, are broader than the atomic lines, see figure 3, and are of similar width to the band width of the output of the diode laser, effectively increasing the absorption

of the pump power, and subsequent lasing of the system. As in DPAL, due to their low cost and their high efficiency in the region that covers the D transition satellites of Cs and Rb¹⁵, diode lasers are a convenient source for the excitation of the alkali metals.

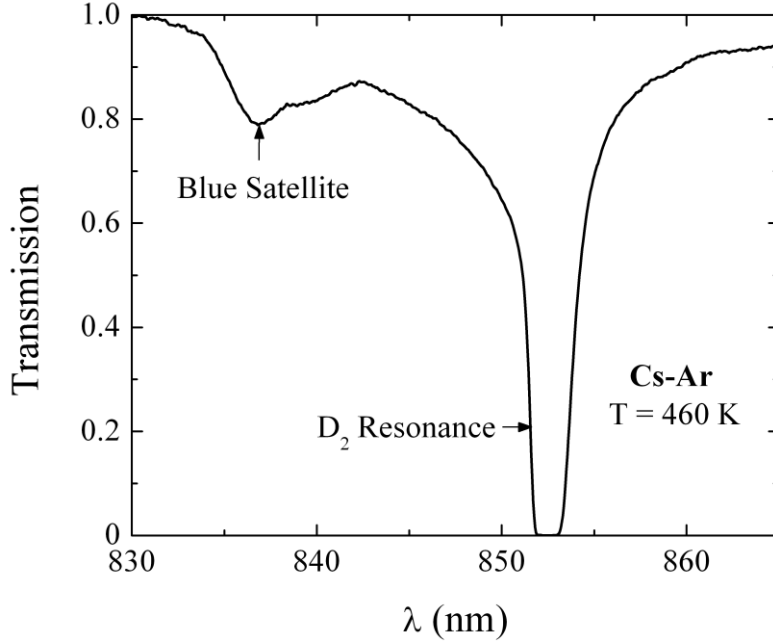


Figure 3: Figure from reference 15, the spectrum covers the atomic transition and the blue satellite of Cs. The blue satellite feature of Rb was also documented in the report from which this figure is extracted.

In order to maximize the overlap of the absorption band with the one of the pumping source, it was originally thought by the Eden group¹⁵ that the satellite absorption band could be shifted by using a mixture of RG atoms, with the absorption band being modeled by a weighted linear combination of the single rare gas absorption coefficients. In a simple model, the absorption of the alkali metal in a mixture of rare gases, denoted by $A_{\text{mixturegases}}(\lambda)$, would be predicted by:

$$A_{\text{mixturegases}}(\lambda) = C1 * A_{\text{buffergas1}}(\lambda) + C2 * A_{\text{buffergas2}}(\lambda)$$

Where $A_{\text{raregas}}(\lambda)$ is the absorption intensity of the alkali metal/single rare gas mixture at a wavelength λ , C1 and C2 are the percentages of rare gas 1 and rare gas 2 respectively, in the mixture. To that effect, mixtures of rare gases have been considered for the laser cell. The

approximation represented in the previous equation was not matched by experimental findings of the Eden group, instead, for the alkali metal in a 50/50 mixture of Ar/Kr, the absorption band had a profile similar to the alkali metal in pure Ar, but, with greater intensity, see figure 4. It is unclear what is causing this behavior, it has been speculated, with the report of these observations, that it could be due to a change in the probability distribution of the atomic distances due to the influence of the collision pairs, or that the dipole moment would be changed by the presence a third body.

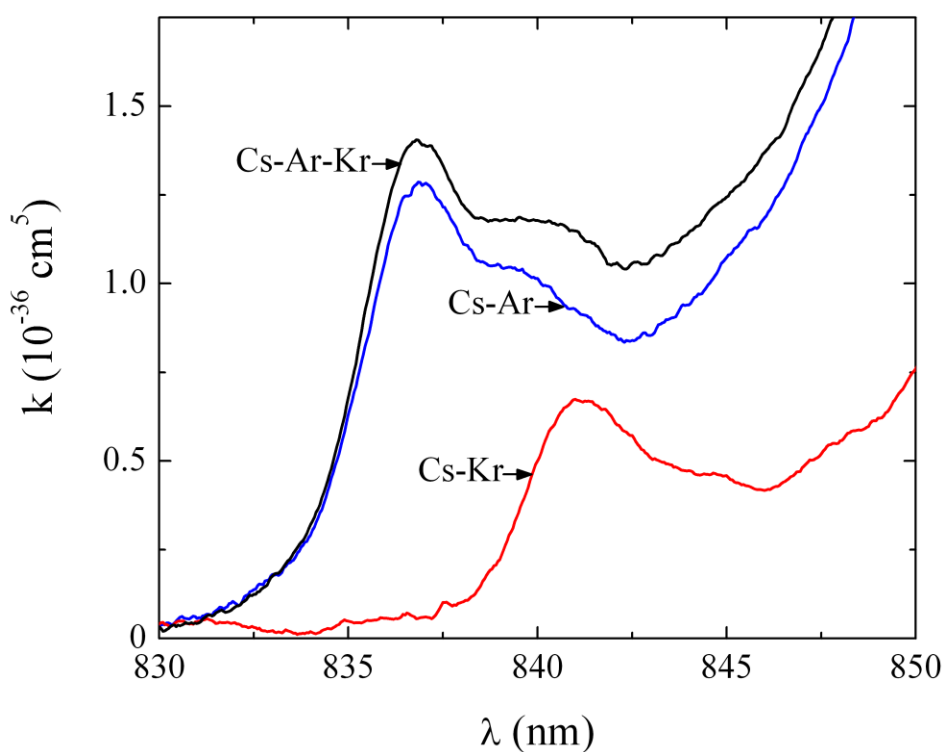


Figure 4: Excitation spectrum in the blue satellite region of Cs with several sets of rare gases. When Cs is present with a 50/50 mixture of Ar and Kr, the blue satellite profile is much more like the one where only Ar is used (blue curve) instead of a combination of the Cs-Ar and the Cs-Kr spectra, fig. from reference 15.

In the mixtures of alkali metal and rare gases, it is not possible to know what the nature of the rare gas atoms that are around the alkali metal atom yielding fluorescence is. In order to investigate the Rb-RG dimers and trimers one would need to employ a supersonic jet

expansion in order to form these complexes. Previous experiments in the Heaven group to that effect have been attempted but were unsuccessful.

A way to circumvent the difficulties associated with studying the interactions of the alkali metal with a mixture of rare gases in the gas phase would be to perform matrix isolation spectroscopic experiments, where the matrix consists of differing mixtures of rare gases. In the solid phase, the probability of having a certain type of a noble gas in the vicinity of the alkali metal could be determined using Monte Carlo Simulations²⁵. By having the spectra of alkali metals embedded in matrices with various mixtures of rare gases and the predictions on the way the rare gas atoms would surround the metal, models could potentially be developed to explain the three body interactions observed. Ryan et al.²⁶ developed a theoretical model to explain the spectral characteristics of the alkali metals in the solid phase using Diatomics in Molecules (DIM) principles. In those, the pair potentials between two rare gas atoms were modeled with a Lennard-Jones potential and the interaction potentials for an alkali metal and a rare gas atom were modeled by fitting experimental interaction potentials of such systems to functions of the form:

$$V(R) = \sum_{k=1}^n a_{2(k+2)} \left(\frac{R_0}{R}\right)^{2(k+2)}$$

Where $V(R)$ is the potential of the two atoms at an internuclear distance R , R_0 is the equilibrium bond distance of the alkali metal-rare gas pair determined experimentally by supersonic jet expansion and $a_{2(k+2)}$ is the least square fit coefficient of the experimental interaction potential associated with the term of degree $2(k+2)$. Ryan et al.²⁶ used the most extensive DIM methods and only one of the three features of the experimental absorption data of a Na-RG matrix could be adequately modeled. Jacquet et al.²⁷ considered three body interactions under the form of induced dipole-induced dipole interactions and computed

excitation spectra comparable to the ones observed experimentally, thus, this set of study would also suggest that three body interactions have a considerable role in XPAL. In order to model the interactions between the alkali metal and the rare gases experimental data on these systems is needed to check the validity of the theoretical models. Matrix experiments previously performed in the Heaven appeared were unsuccessful and it appeared that the metal in its atomic form was not being deposited in the matrix. The gas phase experiments presented in this report would provide heating conditions that lead to vaporizing the metal in its atomic form. Thus, the results from the gas phase experiments here presented could be used to improve the metal vaporization in matrix experiments and lead to the deposition of exploitable matrix samples.

1.4 Multiphoton excitation

As seen in figure 1 and 2, the lasing of the DPAL and XPAL results from the relaxation of Rb^* to its ground state, therefore, it is important to understand the energy transfer pathways of Rb^* . In operating such lasers employing high power pump lasers, the collisional relaxation of the alkali metal will lead to an increased temperature of the cell, specifically in the region that is being pumped. Unintended population of higher lying electronic states or ionization of the metal through multiphoton ionization will also scale with the power, thus, it is essential to know how the population of these levels and metal ionization is affected by the pressures of the buffer gases used in the cell¹⁷.

Experimental data for cesium from Arimondo et al.²⁸ shows that the element is subject to multiphoton absorption when being excited on its D transitions. The ionization of cesium was further investigated by Barmashenko et al.¹⁷ who formulated a kinetic model for an XPAL using cesium and the study showed that photoionization of the metal by continuous wave pumping is followed by an association of the metal ion with a neutral metal atom which then

leads to the dissociative recombination of the ionic dimer. Experimental data for Rb to formulate such models is not available, this work is performed with intention of obtaining data and results that will guide the development of such models.

Experimental work by Cheret et al.²⁹ has shown that the ionization of Rb vapor subjected to continuous wave excitation involves energy pooling (EP). EP is a process in which energy transfer occurs upon the collision of two excited atoms. The Cheret study suggested that a one-photon ionization of the highly excited atom produced from the EP was responsible for the formation of monoatomic Rb ions, a theoretical study by Mahmoud³⁰ later confirmed that model. The same study also showed that the collision of two single excited Rb atoms can lead to the formation of Rb_2^+ , a process labeled as associative ionization. Existing data on an analogous cesium model suggests that the buffer gas plays a role in the formation of the alkali metal dimer ions, however, the role of a buffer gas in the formation of Rb_2^+ was not previously investigated. In the cesium study of Arimondo²⁸, analysis of the data showed that Cs_2^+ dissociates upon recombination with an electron. This dissociation process yields neutral atoms in their excited states and their radiative decay signal was monitored and used to model the kinetics of the ionization process. Similarly, in a Rb-He vapor pumped at 780nm with He pressures between 75 and 150 torr, the observation of a radiation detected at 422 nm, corresponding to the $6p \rightarrow 5s$ transition of Rb³¹, and its buffer gas pressure dependence can be used to gain insight on the kinetics giving rise to the presence of the signal. If the kinetic processes of the Rb system are comparable to the cesium model, this signal is likely the result of a reaction involving Rb_2^+ , in which case these experiments would be the first to study the effects of the pressure of the buffer gas upon the formation of Rb_2^+ in a Rb-RG cell.

In these systems, Rb_2^+ would be a product of a reaction involving Rb^+ . The atomic ion density is determined by the laser power and the metal concentration, however, the association

process of the atomic ion with the neutral metal atom is affected by the density and nature of the buffer gas due to three body collisions. So far, the extent to which these processes contribute to ionization is unknown and determining the kinetics of this unintended ionization process will provide information that will aid to minimize its occurrence in XPAL and DPAL design. A comparable model for cesium²⁸ suggests the occurrence of ionization through consecutive steps taking place after the initial excitation pulse. These experiments provide the data necessary to develop such models for Rb which may in turn be used to minimize the loss of the pumping energy through peripheral processes, such as multiphoton absorption and metal ionization, in alkali metal lasers.

2 Experimental Details

2.1 Vaporization of the metal

The alkali metal was placed inside a hole drilled in a stainless steel rod of a diameter of 5/16" and of about 3" in length. A hole was drilled on the opposite end of the rod in order for a cartridge heater (McMasterr-Carr model 8376T27) to be inserted into it. The voltage flowed through the cartridge heater was adjusted with a variable autotransformer using a standard 110V connection, see figure 4 for a schematic of the vapor source. Typically 50% of the maximum voltage was needed to get a vapor pressure of the metal leading to a substantial signal, the voltage was increased slowly to allow the rod to heat more uniformly and prevent abrupt heating of the Rb that may have caused the metal to violently boil outside the hole where it was placed. Prior to vaporizing the metal, the chamber and its connected components were evacuated by a Welch Duo Seal vacuum pump to 30 mtorr. In experiments using a buffer gas, the gas was flowed through the glass tube containing the vaporizing source and its flow was adjusted so that the pressure of the buffer gas inside the chamber was of about 100 torr prior to heating the metal.

2.2 Laser induced fluorescence

A Quanta-Ray DCR Nd:YAG laser was used to produce 532 nm radiation, which was subsequently used to pump a pulsed dye laser, Quanta-Ray PDL-2 with the dye LDS-768. The pulse duration was 10 ns and its repetition rate was 10 Hz. The beam diameter at 780nm was 2.5 mm and the average beam power was 5mW. The output beam was directed in the chamber where the alkali metal vapor was present. Scattering of the laser light was minimized by passing the beam through baffle arms connected on each side of the chamber. The diameter of the orifices on the baffle arms was about 5 mm.

Fluorescence from the alkali metal induced by the laser beam was detected perpendicularly to the beam. The wavelength of fluorescence transmitted to the detector was selected with a monochromator (Oriel 77250) set for a resolution of 0.3 nm and the light was detected with a photomultiplier tube (PMT), Hamamatsu model R889, subjected to a voltage of 1100V and placed behind the exit slit of the monochromator. The fluorescence signals were recorded with a Yokogawa Digital Oscilloscope with a sampling rate of 150MHz, after which they were transferred to a computer for data analysis, see figure 5 for a schematic of the experimental set-up.

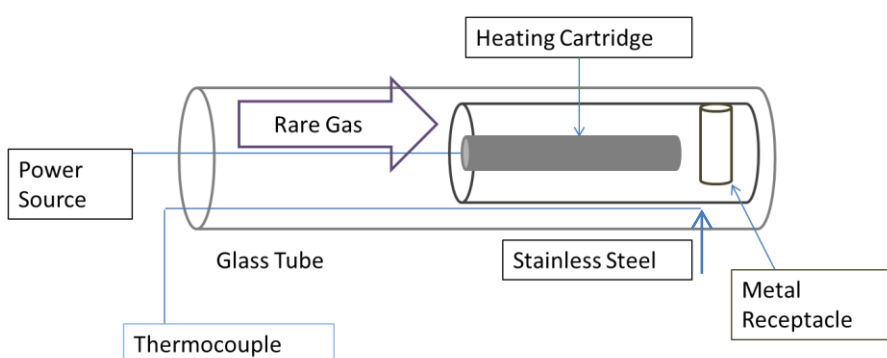


Figure 4: Detailed view of the metal vaporizing source, on the end of the stainless steel rod closest to the beam path, a hole was drilled for the alkali metal to be placed in, marked as the metal receptacle on the figure. On the other end of the rod, a removable heater cartridge was inserted and was used to heat the alkali metal through the rod. The thermocouple (type E) probe was pinched between the stainless steel rod and the glass tube. The length of the tube was about 5", the thermocouple and electrical wires and were passed out of the apparatus through a T-connection and were sealed onto it with Torrseal.

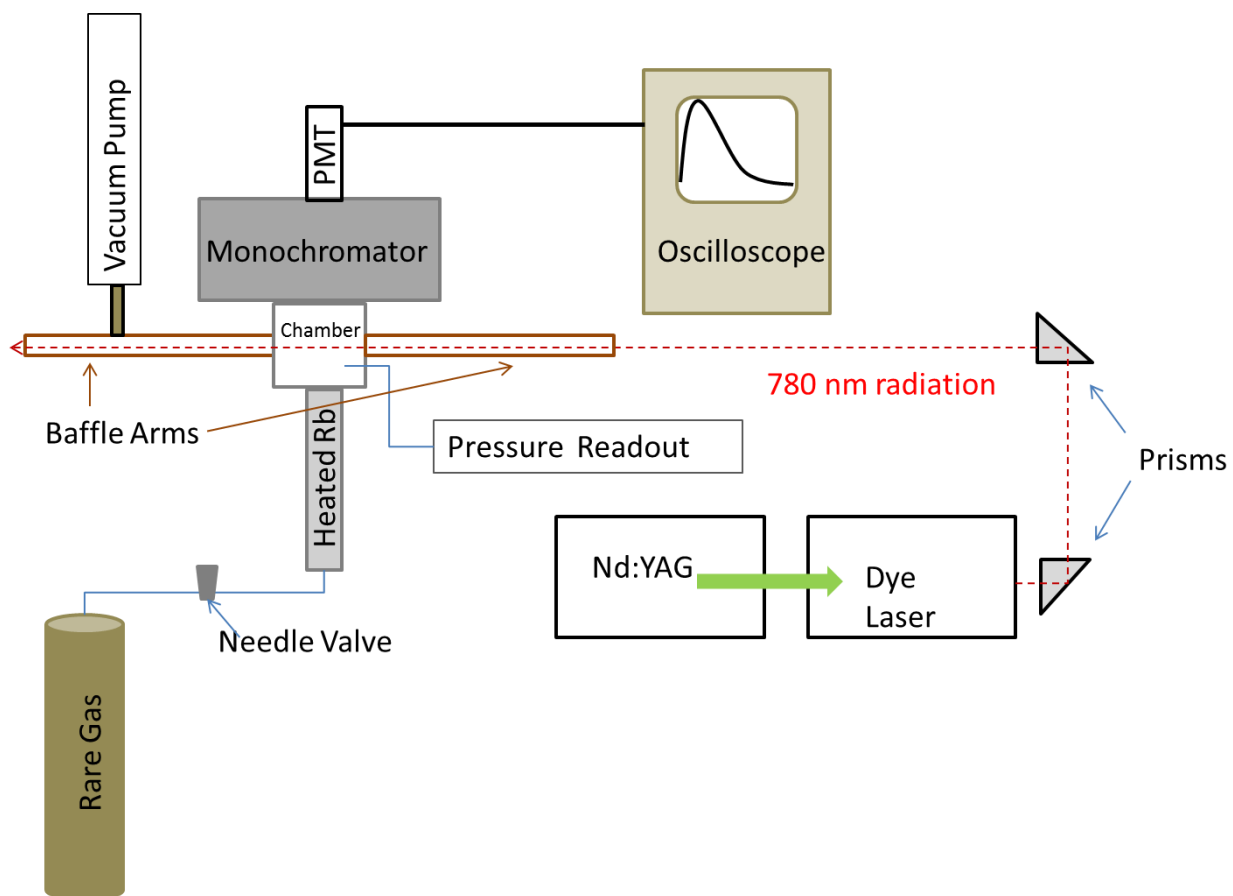


Figure 5: Experimental set-up. The chamber was evacuated and the pressure of the rare gas was adjusted to the pressure desired for the initial experiment. Once reached, the heating source of the metal was increased manually at a rate of about 30V/hr to the point where sufficient atomic signal was detected (50-60 volt on heater cartridge). The 532 nm light from the Nd:YAG laser pumped the dye laser (PDL). The beam from the PDL was visible and crossed the chamber coaxially with the baffle arms, its average power was 5mW. The buffer gas pressure was changed by controlling the needle valve and/or choking the pump line. Fluorescence was detected perpendicularly to the axis of the excitation beam with a PMT connected to an oscilloscope, wavelength selection of the fluorescence detected was done with a monochromator placed before the PMT.

3 Discussion and Results

3.1 Sodium

3.1.1 Preliminary testing of the system

As a way to test the apparatus, sodium was vaporized and its D lines were sought. The decay rate of the fluorescence from the D₂ line at various gas pressures of He and Ar was recorded in order to compare it with the one reported in the literature. The output of the dye laser was calibrated using a wavemeter (Bristol 821 Pulsed Wavelength Meter). The sodium D transitions were then found by scanning the dye laser and removing the monochromator from the scheme shown in figure 5. The spacing between the D lines obtained was 0.5 nm which is in agreement with the spacing of 0.53nm reported in literature³². The D₂ line is more intense than the D₁ line due to the higher degeneracy of the ²P_{3/2} state, see fig. 6.

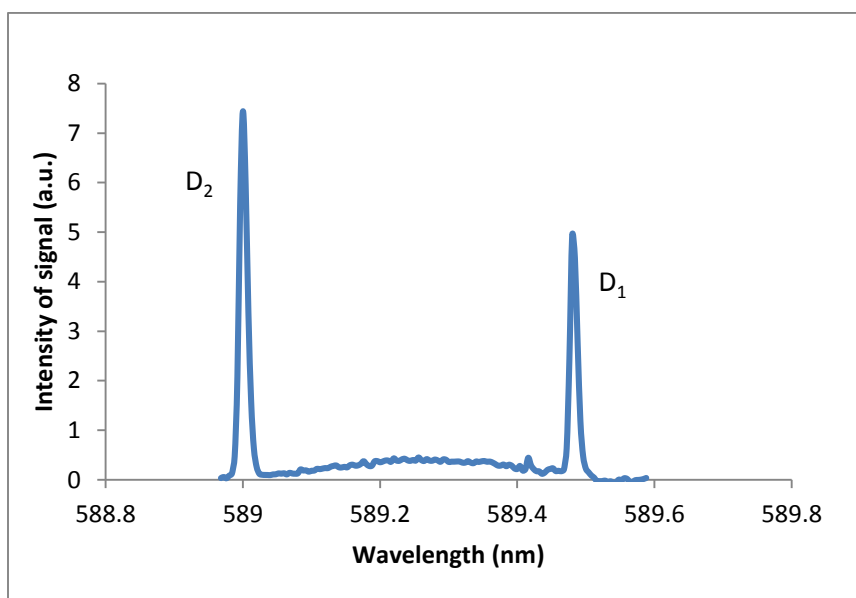


Figure 6: Laser Induced Fluorescence spectrum of sodium in the region covering the D-lines. For this spectrum the sodium was heated to 260°C and no buffer gas was used.

3.1.2 Fluorescence decay time

Since the pulse duration of the laser is on the same order of magnitude as the decay time of the D lines fluorescence of sodium, the decay curves (see figure 7 for a representative decay curve) were fit with the Origin Software to a sum of two exponential functions, see equation 1, yielding two decay times. The shorter decay time is associated with the pulse of the laser while the longer decay time is associated with the fluorescence signal subjected to radiation trapping.

$$I(t) = y_0 + A_1 e^{-\frac{t}{\tau_1}} + A_2 e^{-\frac{t}{\tau_2}} \quad \text{equation 1}$$

Where y_0 is the baseline level of the signal, A_1 and A_2 are constants determined by the fitting, τ_1 and τ_2 are the decay times obtained from the fitting.

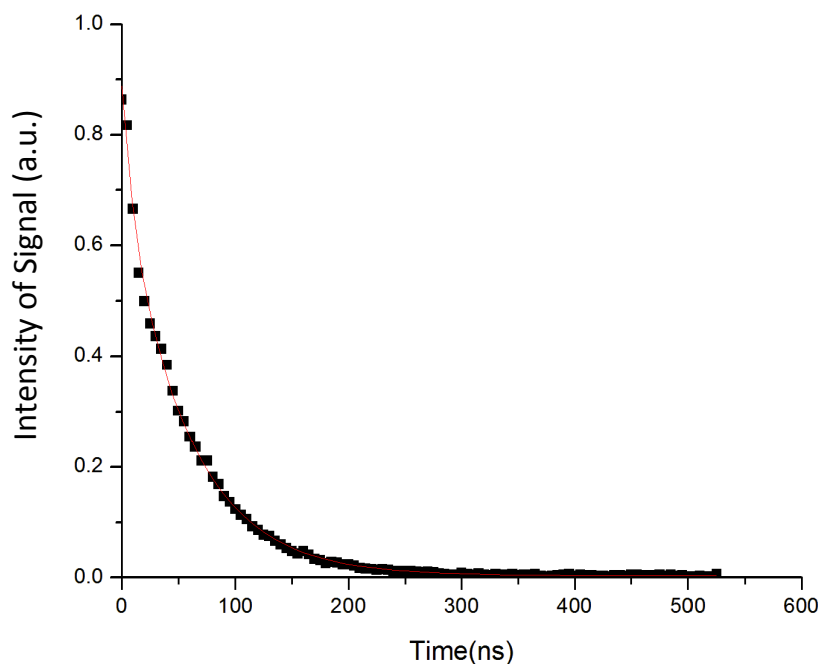


Figure 7: Time based signal of Na fluorescence excited and detected at 589 nm, the black squares are the experimental points and the red curve is obtained from the fitting of the signal to equation 1.

Radiation trapping refers to the process in which a photon is absorbed and emitted several times by the atoms or molecules studied before it is detected²². If the alkali metal density is high enough, a photon emitted by the alkali metal will encounter other metallic atoms in the vapor that are in their ground electronic state, and the photon will be subject to reabsorption. Thus, before a photon reaches the PMT, it may have undergone several absorption and emission cycles, which will result in an increase of the lifetime of the signal detected. Radiation trapping effects are increased with an increased density of the absorbing species and by increasing the path length between the radiation source and the detector.

Gas	Pressure (torr)	Lifetime (ns)	Intensity of the first point (a.u)	Temperature (°C)
He	4.4	28.46	7.31E-02	277
He	5.45	27.34	1.63E-01	271
He	6.31	26.71	3.38E-01	274
He	7.67	24.61	8.82E-01	279
He	10.2	24.01	7.23E-01	274
Ar	4.93	19.20	4.90E-02	274
Ar	6.29	26.82	9.76E-02	275
Ar	7.47	26.06	1.78E-01	273
Ar	8.68	25.00	3.35E-01	277
Ar	10.05	25.50	6.71E-01	275

Table 1: lifetime of laser induced fluorescence of Na vapor at 589.0 nm. Curves were recorded for various pressures of Ar and He between 4 and 11 torr. The lifetime of the fluorescence does not appear to depend on the pressure of the buffer gas.

Radiation trapping effects are detected in this set of experiments by an increase in the lifetime of the fluorescence observed when compared to the one reported in existing reports. The signal detected here corresponds to the transition of an electron from the $A^2P_{3/2}$ to the $X^2S_{1/2}$ electronic states of sodium. The lifetime of the $A^2P_{3/2}$ state of sodium reported in the

literature is 16ns³³. All of the decay times measured lie within a factor 2 of that lifetime and this difference is likely a result of radiation trapping. The transport of the metal into the beam path depends on the flow of the buffer gas, which is increased as the pressure of the buffer gas is increased. The buffer gas will entrain more metal atoms as its flow is increased. This is observed in this set of data by an increasing intensity of the signal as the buffer gas pressure is raised, small deviations from that trend could be due to small changes in the vapor pressure of the metal. This simple testing of the apparatus, which used sodium due to its easier handling compared to other alkali metals, was satisfactory and did not raise technical concerns that would complicate the observation of fluorescence from Rb, which is of interest due to its potential use in XPAL and DPAL. This experiment also provides information on the settings necessary to produce amounts of metal vapor that would lead to detection of the alkali metal signal when placed in a matrix sample. Next, the system was used with 40-100 torr pressures of buffer gas, which is closer to the pressure range needed for DPAL and XPAL design.

3.1.3 Variation of the buffer gas pressure spanning 40-100 Torr

One of the objectives of this experiment is to provide details on how the multiphoton ionization process is affected by the nature of the buffer gas. To that effect, the D₂ line fluorescence decay of sodium was studied in He and Ar. As seen in table 2, at similar metal vapor densities, the lifetime of the fluorescence increases as the atomic weight of the buffer gas is increased: the lifetimes for Ar are larger than the ones observed for He by more than a factor of 2. The pressure broadening coefficient of argon is smaller than the one for helium, 17.7 MHz/Torr vs. 20 MHz/Torr for helium³⁴. At 100 torr of buffer gas pressure, this would correspond to band width of about 2GHz and the band width of the laser used is on the order of 10²-10³ GHz. Thus, with Ar as the buffer gas, a larger population of the alkali metal atoms is able to absorb the photons used in the excitation, resulting in a larger radiation trapping

effect and consequently a larger observed decay time of the signal. The following equations were developed for cesium by Brown and Perram²² and describe how the trapping coefficient, ζ , which is the observed decay rate of the signal divided by the rate of the transition considered, is related to the population density of the metal:

$$\zeta = \frac{1}{A * t_2} = \frac{1.115}{\sqrt{\pi k_p r}} \quad \text{equation 2}$$

Where k_p is defined by:

$$k_p = \frac{N_0 \lambda^2 g_u A}{2\pi g_e \gamma_p} \quad \text{equation 3}$$

In these equations: t_2 is the decay time of the signal observed obtained from equation 1, its inverse divided by the Einstein coefficient of the transition considered A , is the trapping coefficient ζ . ζ was “defined as the number of times a photon is absorbed after traveling a distance r before being emitted”²² while it is in fact the mathematical inverse of that definition, g is the degeneracy of the energy level l , N_0 is the number of metal atoms per unit of volume, λ is the wavelength resonant with the transition, γ_p is the pressure broadening factor and r is the path-length of the trapped photon (from the beam center to the window of the chamber).

Gas	Pressure (Torr)	Lifetime (ns)	Metal Density (atoms/cm ³)	Area under Curve (a.u)	Predicted $\tau(\text{He})/\tau(\text{Ar})$	Experim. $\tau(\text{He})/\tau(\text{Ar})$	Percent Difference
He	40.8	56.19	1.70E+10	44.03	0.50	0.39	29.26%
He	70.8	61.04	3.47E+10	77.21	0.67	0.45	49.16%
He	100	62.39	4.53E+10	94.85	0.64	0.45	44.19%
Ar	39.8	144.96	9.74E+10	81.65	N/A		
Ar	76	135.27	1.62E+11	111.81			
Ar	103	139.5	2.33E+11	140.43			

Table 2: Population density and fluorescence lifetime of Na at 589nm in Ar and He within 39-103 torr pressure of buffer gas, a representative curve for which the area underneath is integrated can be found in figure 7.

Using equation 2 and 3, an inverse square root dependence of the pressure broadening coefficient on the lifetime is deduced, using that dependence, and using the metal density ratio between the two rare gases determined from integration of the decay curve over the fluorescence decay time, $N_0(\text{He})/N_0(\text{Ar})$, the predicted ratio of the fluorescence lifetimes for Na in a He or Ar buffer medium, $\text{Pred.} \frac{\tau(\text{He})}{\tau(\text{Ar})}$, is calculated by:

$$\text{Pred.} \frac{\tau_{\text{He}}}{\tau_{\text{Ar}}} = \sqrt{\frac{\gamma_p(\text{Ar}) * N_0(\text{He})}{\gamma_p(\text{He}) * N_0(\text{Ar})}}$$

where $\tau(\text{He})$ and $\tau(\text{Ar})$ are the decay times of the signal observed, denoted as t_2 in equation 1 and 2 between 0.50 and 0.67, these match the observables within 50%, see table 1, the percent difference was obtained by:

$$\%Difference = \frac{\text{Pred.} \frac{\tau(\text{He})}{\tau(\text{Ar})} - \text{Exp.} \frac{\tau(\text{He})}{\tau(\text{Ar})}}{\text{Exp.} \frac{\tau(\text{He})}{\tau(\text{Ar})}} * 100$$

The denominator was chosen to be the experimental ratio since it was a smaller figure and would lead to an upper bound on the error.

3.2 Rubidium

After checking the system with sodium, the experiments shifted towards rubidium in order to study some of the processes that occur as the atoms are excited on their D_2 transition. The objective of this experiment was to establish the kinetics of an observed transition detected around 422nm when the atom is excited on its D_2 line. Similar experiments were previously performed in the Heaven group, but the expensive vapor source used at the time limited the variation of the experimental settings that could be tested and the EP process assumed could not be verified. With the set-up used in the present study, the pressure of the buffer gas could easily be adjusted and sufficient data was collected in order to present a model explaining the observation of the 422nm signal.

3.2.1 Determination of the metal vapor density

To model the kinetics of the aforementioned process, it is necessary to determine the concentration of the metal in the vapor. Although the temperature to which the metal was heated was recorded, the vapor density of the metal in the apparatus could not be reliably obtained from it. This because the metal density in the beam path of the laser is dependent on the transport of the metal by the carrier gas and this dependence has not been quantified. However, a model recently developed by Perram and Brown²² correlating the vapor density of a metal with the decay time of its fluorescence subjected to radiation trapping, was used to determine the metal vapor density. Since radiation trapping was evident from the decay

curve of the fluorescence from the metal, the Perram and Brown model was used to determine the density of the metal based on the lifetime of its fluorescence. Equations 2 and 3 quantify that model and together these equations can be used to estimate the metal vapor density from the lifetime of the fluorescence at 780 nm. The 780 nm fluorescence is obtained by pumping the alkali metal from the $5^2S_{1/2}$ ground state to the $5^2P_{3/2}$ state. Consequently, the electron in the excited state will decay to the ground state which will emit a radiation through fluorescing. The trapping lifetime of the fluorescence emitted is used to determine the population density of the metal. Also, when He is present, it will induce relaxation to the $^2P_{1/2}$ state, causing a loss in the fluorescence intensity in resonance with the excitation.

For the first set of excited P states of the alkali metal, the rate at which the spin states, R_{21} , of the excited alkali metal are mixed, called the mixing rate, is temperature dependent, and is defined by³⁵:

$$R_{21} = \langle \sigma_{21} \rangle * n_{bgas} * \bar{v}$$

Where $\langle \sigma_{21} \rangle$ is the velocity averaged collisional transfer cross section from spin state 2 to 1, n_{bgas} is the population density of the buffer gas and \bar{v} the average velocity of the colliding pairs and is computed by:

$$\bar{v} = \sqrt{\frac{k_B T}{\pi \mu}}$$

Where k_B is the Boltzmann constant, T is the temperature of the system and μ is the reduced mass of the colliding pair.

Quenching of the excited states of Rb to the ground electronic state by the buffer gas is negligible since the corresponding rate constants are on the order of $10^{-13} \text{ cm}^3\text{Hz}$ ³⁶, which is several orders of magnitude below the ones for the kinetic model considered.

The ratio of the mixing rates for the spin orbit states can be calculated with the following equation:

$$\frac{R_{12}}{R_{21}} = \frac{g_2}{g_1} e^{-\Delta E/kt}$$

Where R_{12} corresponds to the rate at which the atoms are transferred from the lower spin state $^2P_{1/2}$ to the higher spin state $^2P_{3/2}$ and R_{21} corresponds to the reverse process. Between the two spin states of Rb this ratio was 0.63 at 300K, meaning that, at equilibrium conditions, 38% of the atoms absorbing the trapped radiation could emit on the D_1 line, at 795 nm instead. At the time the experiments were performed this effect had not been considered and this paper offers no report of the fluorescence from the D_1 line upon D_2 excitation, however, with the metal densities used in these experiments the mixing rate is 10^6 Hz or 100 times smaller than the ionization rate, thus the mixing effects are not likely to contribute significantly. To confirm that prediction, future experiments should include the detection of fluorescence signal on the D_1 line to verify that the effects of mixing in this set-up are negligible. If it unexpectedly turns out that the D_1 fluorescence is significant upon pumping the D_2 line of Rb, models considered will have to include these effects to correctly depict the population density of the metal.

The decay rate of the trapped radiation depends on the type of broadening governing the experiment. At the pressures of the buffer gas, p , used in these experiments (50-150Torr) and at 300K, the pressure broadening, at the Full Width at Half Maximum (FWHM), $\Delta\vartheta_p$, has the largest broadening effect when compared to Doppler broadening at the FWHM, $\Delta\vartheta_D$:

$$\Delta\vartheta_D = 2\vartheta_0 \sqrt{\frac{2k_B T \ln(2)}{mc^2}}$$

$$\Delta\vartheta_p = bp$$

Where ϑ_0 is the frequency of the atomic transition, T is the temperature, k_B , the Boltzmann constant, m is the mass of the absorbing atom, c is the speed of light and b is the pressure broadening coefficient. At 300K and at 50 torr $\Delta\vartheta_D = 0.6\text{GHz}$ and $\Delta\vartheta_p = 1\text{GHz}$ and for the same temperature at 150 torr, $\Delta\vartheta_D = 0.6\text{GHz}$ and $\Delta\vartheta_p = 3\text{GHz}$, so, assuming that the broadening is done primarily by pressure broadening is a reasonable approximation and the constants associated with pressure broadening trapping coefficient, ζ , defined by equations 2 and 3 are used.

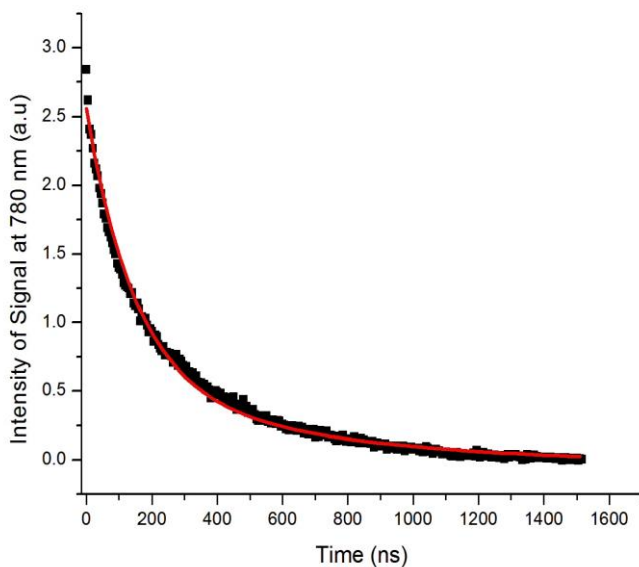


Figure 8: Decay curve of the 780nm fluorescence from Rb excited by 780nm radiation. The red line is the curve associated with the fitting of the data points (in black) to the form shown in equation 1. The fluorescence decay curves at various gas pressures were systematically fitted to extract the fluorescence decay rate which was then used to determine the metal vapor density.

As a way to assess the validity of the metal density obtained based on the decay time of the fluorescence signal at 780nm (D_2 transition), the ratios of the metal vapor densities calculated

using the trapping model were compared to the ratios of the metal vapor pressures obtained from the temperature to which the metal was heated, p_{mm} calculated from³⁷:

$$\log_{10}(p_{mm}) = \frac{-A}{T} - B * \log_{10}(T) + C - D * T \quad \text{Equation 4}$$

Where p_{mm} is the vapor pressure of the metal in millimeters of mercury, T is the temperature of the metal in K, and A, B, C and D constants specific to the metal of interest, these are reported to be 1961.258, -42.575, -94.04826 and 0.03771687 respectively³⁷. Since a higher vapor pressure of the metal means that more metal atoms will be vaporized, the ratio of the vapor pressure of the metal between different experimental samples is indicative of the ratio of the metal vapor density between these samples. This allows the use of the vapor pressure of the metal as a tool to assess the coherence of the metal vapor densities calculated.

Each time-based curve for the 422nm fluorescence was associated with a decay curve of the D₂ fluorescence at 780 nm, recorded directly prior to setting the monochromator to that wavelength, allowing for the determination of the metal vapor density through radiation trapping, and a temperature measured in the proximity of the stainless steel rod, indicative of the one of the metal, allowing for the calculation of the metal vapor pressure. These two parameters, concentration of the metal from radiation trapping and metal vapor pressure, provide two independent ways of estimating the relative metal vapor density between two experimental samples. Thus, the agreement of the relative metal density using the two methods would provide some confidence with regard to the validity of the metal densities calculated. The comparison between the relative metal densities was quantified with equation 5.

$$\text{Ratio for vapor pressure}(x, y) = \frac{p_{mm}(x)}{p_{mm}(y)}$$

$$\text{Ratio for trapping}(x, y) = \frac{N_{\text{trapping}}(x)}{N_{\text{trapping}}(y)}$$

$$\text{Ratio}_{\text{density/vapor pressure}}(x, y) = \frac{\text{Ratio for trapping}(x, y)}{\text{Ratio for vapor pressure}(x, y)} \quad \text{Equation 5}$$

Where x and y can represent any unique set of two experimental samples, N is the population density of Rb obtained from the lifetime of the signal and p_{mm} is the vapor pressure of the metal based on the temperature recorded for the sample curve. Over all pairs of experimental samples, each experimental sample being associated with a vapor pressure of the metal and a metal vapor density, the average deviation from 1.00 of the ratio of the metal density over the metal vapor pressure, $\text{Ratio}_{\text{density/vapor pressure}}$, was 0.32, value obtained from a program written in Python. This value suggests that the method to calculate the metal vapor density is sensible.

3.2.2 Fluorescence at 422 nm from Rb when pumped on its D_2 transition

Rb in the gas phase has been shown to have pumping efficiencies up to 0.5% for the emission from the 6p to the 5s level upon two photon absorption processes resonant with transitions from the 5s to the 5d orbitals³¹. The metal vapor density in those experiments was on the order of 10^{15} atoms/cm³ and the system contained no buffer gas. The same emission was observed in these experiments and a model is presented in an attempt to define the kinetics of this process.

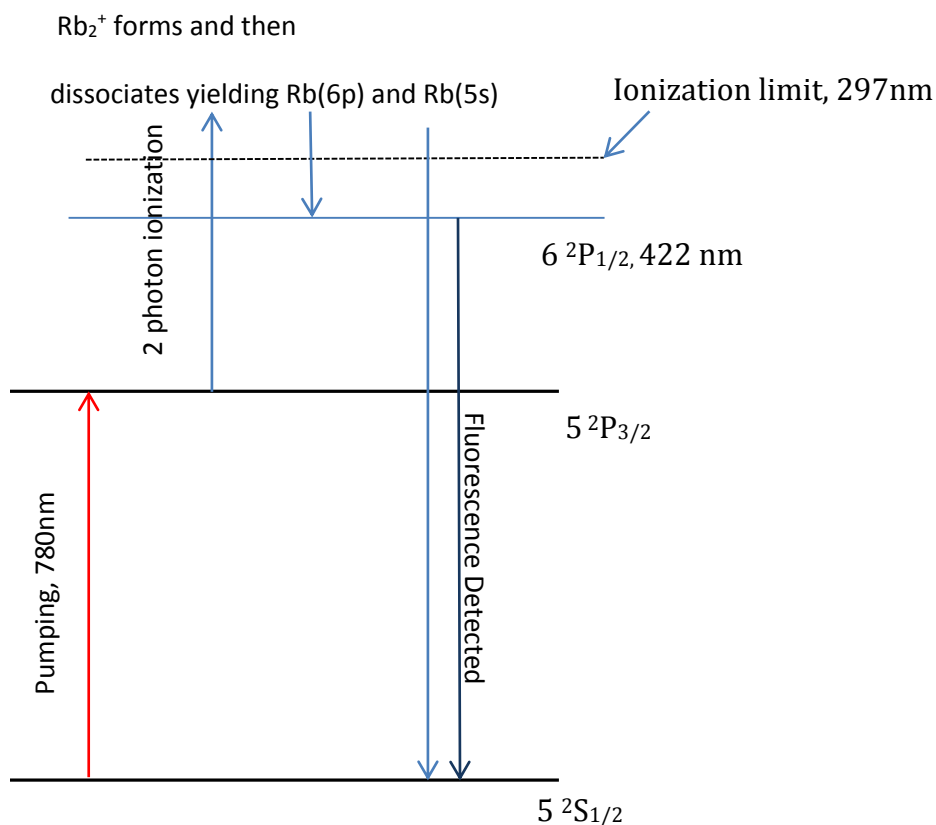
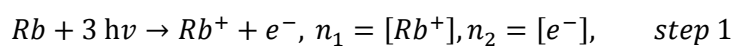


Figure 9: Simplified diagram of the transitions involved in exciting the Rb vapor with 780 nm radiation. The Rb atoms are ionized through a 3 photon process, one to pump the valence electron to the $^2P_{3/2}$ state and two to ionize it from that level, a 1+2 photon process; the high powers used in this experiment makes this feasible. Once the Rb is ionized, the ion undergoes a collisional process to form the metal dimer ion which upon dissociation yields Rb(6p) and Rb(5s), the radiative decay from the 6p state is then detected at about 422nm.

With the instantaneous MW power used in this experiment, I_{power} , calculated using:

$$I_{power} = \frac{\text{Average Laser Pulse Power}}{\text{Laser Pulse Duration}}$$

Rb could be ionized by the following multiphoton process:

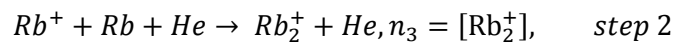


The rate of ionization, R_I was calculated to be $1.3 \cdot 10^8$ Hz with the following equation:

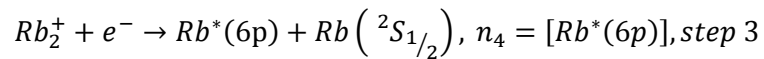
$$R_I = \frac{P_{beam} * \sigma_{ionization}}{A_{beam} * E_{780nm\ photon}}$$

Where P_{beam} is the instantaneous power of the beam, $\sigma_{ionization}$ is the cross section of ionization at 780nm from Mahmoud³⁰, A_{beam} is the area of the beam cross section and $E_{780nm\ photon}$ the energy of one photon with a wavelength of 780nm. R_I is on the same order of magnitude as the pulse duration and the other processes considered have much lower rates, so, the ionization step is considered to be instantaneous.

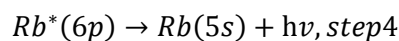
The metal ion present in the gas phase may then undergo an association reaction, with a neutral metal atom, possibly found in the vapor surrounding the beam path when the ionization takes place, forming a metal molecular ion:



In the above equation He takes away the energy released in the formation of the Rb dimer. Once the dimer is formed, it would recombine with an electron produced from the ionization of the metal and dissociated into two neutral atoms:



Finally the excited Rb neutral undergoes a radiative decay, whose radiation is detected:



Step 2 is the rate limiting step of the process. According to the reaction steps described above, the following equations for the population densities were used to model the decay form of the 422 nm signal:

$$\frac{dn_1}{dt} = -\Gamma n_1, \text{ where } \Gamma = k_1[\text{Rb}][\text{He}]$$

$$\frac{dn_2}{dt} = -k_2 n_2 n_3$$

$$\frac{dn_3}{dt} = \Gamma n_1 - k_2 n_2 n_3$$

$$\frac{dn_4}{dt} = k_2 n_3 n_2 - k_3 n_4$$

The initial conditions for the population densities were:

$n_1(0) = n_2(0) = [\text{Rb}]$, this because all the metal atoms in the beam path are assumed to be ionized with the high power beam, n_3 represents the molecular ion and it is formed by a slow process, so $n_3(0) = 0$ and since n_4 requires n_3 to be formed in this model $n_4(0) = 0$.

$[\text{He}]$ was determined through the ideal gas law, the temperature used for its computation was the one of the system, taken to be 298K and the pressure used was the one detected inside the chamber. The pressure inside the chamber was a good approximation of the one of the buffer gas since in the absence of the buffer gas, the chamber pressure was below a torr and was at least of 45 torr when the buffer gas was present.

$$[\text{He}] = \frac{n(\text{He}) * N_A}{\text{Volume of Apparatus}} = \frac{P * N_A}{RT} \quad \text{equation 6}$$

Where N_A is the Avogadro's number, P is the pressure inside the chamber, T is the temperature of the apparatus and R is the ideal gas constant. $[\text{Rb}]$ was determined from the decay rate observed on the fluorescence of the D_2 line. The recombination coefficient between the dimer ion and the electron k_2 was set to $1.0 * 10^{-5} \text{ cm}^3 \text{ Hz}$, the corresponding coefficient for the cesium system was reported to be $1.0 * 10^{-7} \text{ cm}^3 \text{ Hz}$ ²⁸. Whereas in the cesium study, the diffusion of the electron was taken into account in the model to obtain the rate

constant, it was not so in these experiments since no electrodes were used to collect the charges. The necessity of the usage of a higher rate constant may be explained by this discrepancy. The rate constant, associated with the radiative decay of the 5p state of Rb has been reported to vary with the buffer gas pressure due to the quenching it induces³⁶. In that model the effective rate, denoted as k_3 here, varies linearly as a function of the buffer gas pressure. The rate constant and factor of the buffer gas pressure, k , is associated to the rate of the transition without quenching. The same model was used to estimate the quenching effect of the buffer gas pressure on the radiative decay of the 6p state. The reported transition rate of the 6p→5s fluorescence is $8 \cdot 10^6$ Hz³⁸, however, due to radiation trapping the observed rate is smaller than the one in the literature. Using equation 2 and 3, the rate taking into account radiation trapping, k , was estimated. Thus, the effective rate, k_3 , was determined with the following equation:

$$k_3 = k + k[\text{Rare Gas}]$$

$$k_3 = 3.0 \cdot 10^{-6} + [\text{He}] \cdot 3 \cdot 10^{-6} \text{ cm}^3\text{Hz}$$

It will be noted that the experiment referring to the study that investigated the quenching effects used alkane gases as the buffer gas and the mixing rates between the spin orbit states had to be considered, since these experiments used He, the mixing rate is not as considerable and is not taken into account to model the quenching effects.

A numerical model of the decay curves, with the discussed conditions for n_1 - n_4 specified, was written in a Mathematica file. The collisional rate constant k_1 was adjusted to maximize the overlap of the modeling curve to the experimental curve. Within 75-154 Torr, with the set of kinetic equations presented for n_1 - n_4 , all of the decay curves could be modeled by varying k_1 within the same order of magnitude. At lower pressures, the intensity of the signal was very weak and modeling of the data could not be performed, this clearly illustrates the dependence

of the 422nm emission on the buffer gas and the feasibility of the kinetics process herein described.

He Pressure (Torr)	99	116	133	154	89	75	100	116	133	154
Temperature of Rb(°C)	131	123	123	124	129	119	131	124	125	125
Metal Density *10 ¹¹ (atoms/cm ³)	17.2	11.2	8.59	10	18.9	9.75	14.1	10.5	8.06	8.01
k ₁ *10 ⁶ cm ⁶ Hz	2	4.5	8	8.3	1.8	9.5	2.5	5	8.5	9.5

Table 3: Settings tested for detection of 422nm radiation of Rb in various pressures of He, the order of the pressures of He listed (from left to right) is respective of the chronological sequence in which the settings were applied. The metal density is the one determined from the fluorescence decay time at 780nm using equations 2 and 3; k₁ is the rate constant associated with step 2 that was found to model the curve well by visual inspection, its variation between the samples could be explained by a slower diffusion of the ions when higher pressures of He are used. The ions would diffuse more slowly at higher pressures, resulting in an increased value for k₁ to compensate that effect. However, the high value of k₁ found at 75 torr does not follow that trend, this may be related to the proximity of that pressure to the pressure threshold of He for which the occurrence of the 422nm fluorescence was detected.

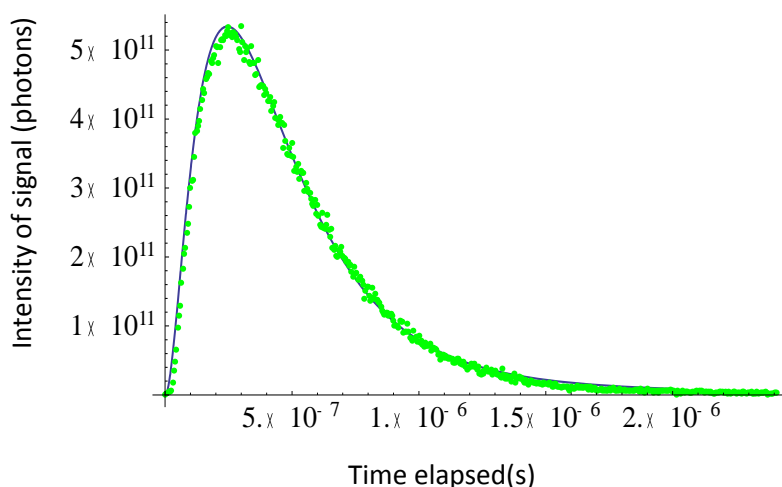
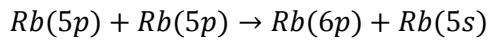


Figure 10: Sample time based signal of radiation of 422 nm when exciting Rb at 780 nm, this curve was recorded with 89 torr of He pressure. The green dots represent the experimental data points while the blue line is obtained from the model presented.

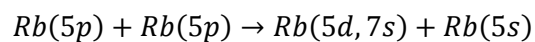
Another way to populate the 6P level would be through energy pooling (EP). In EP, two singly excited atoms collide to form one ground state atom and one doubly excited. In this instance the EP process would be the following:



The rate equation corresponding to the population of the Rb(6p) in this process is described by:

$$\frac{dn_4}{dt} = kn_5^2 - k_3n_4$$

Where k is the rate constant of the EP process $n_4=[Rb(6p)]$ and $n_5=[Rb(5p)]$. Energy pooling processes for Rb have been reported with rate constants, k_{pe} around 10^{-9} - $10^{-10}cm^3Hz$ ^{39,40,41}. The product of this process would be a Rb atom with its valence electron in the 5d or 7s orbital, however, the 6p level could still be populated from relaxation of these states. This process was studied by Perram et al.³¹ and the lifetime of the electron in the 7s and 5d orbitals, denoted by τ subsequently, are respectively around 90 and 250ns⁴², which would correspond to rates of 0.040 to $1.1 \cdot 10^8$ Hz, so, in the EP scheme the rate limiting step would be the one associated with the following reaction:



The EP pooling process has incompatible features with current experimental observations. Firstly, it is dependent upon the Rb being excited to the 5p state, thus, the EP process will cease to occur as soon as the 5p level is depopulated. The 5p state relaxes quickly to the ground state, this would limit the rise time of the signal associated with the EP process to a few tens of ns. The rise time of the signals recorded in this report are of about 200 ns, see figure 11, which is in disagreement with the ones that would correspond to the EP process.

Secondly, in the settings used here, the rate of the EP process is on the order of 10^4 Hz, so, within the timeframe where the Rb 5p orbital population is considerable the EP pathway will be severely limited due to its slower rate. This is seen upon modeling the decay curves at 422nm with the EP model where the population densities of the metal obtained from the model have to be multiplied by a factor of 10^3 to be brought back to scale with the metal vapor densities determined from the radiation trapping. Finally, the EP model makes no provision for the role of the buffer gas, the results presented here show a strong dependence of the signal of the blue fluorescence on the buffer gas pressure with decrease of the signal intensity as the buffer gas pressure decreases, including its disappearance at pressures of 62 torr, see figure 11. If the EP model was the source of this blue fluorescence, the signal would remain constant as the buffer gas pressure is changed, which is in clear disagreement with the current observations.

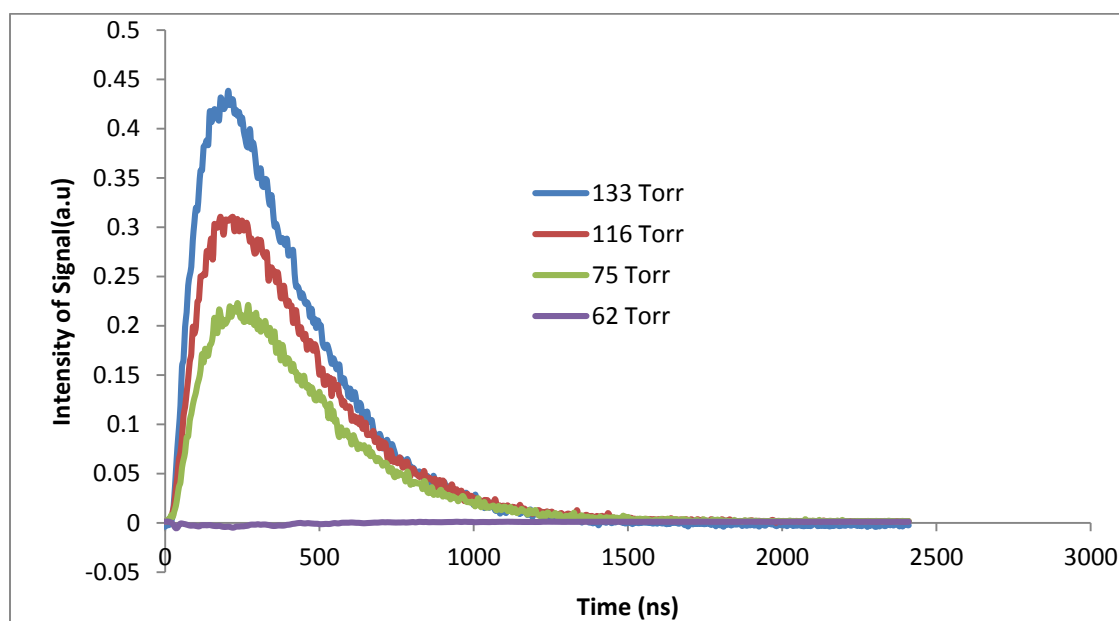
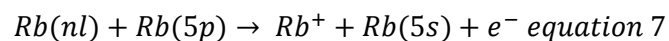


Figure 11: Fluorescence at 422 nm from excitation at 780 nm of Rb at mixed with He as a buffer gas at differing pressures. The intensity of the signal increases with increasing buffer gas pressure. The rise time of the signal can be seen to be of about 200ns. With a buffer gas pressure of 62 torr, the signal is inexistent.

Aside from the formation of monoatomic ions by photoionization, Mahmoud³⁰ developed a model in which the ions could be formed by Penning ionization in which one of the species is a highly excited Rb atom according to the following reaction:



The rate constant of these processes (several excited state levels populated) is on the order of $10^{-8} \text{ cm}^3\text{s}^{-1}$. This process would follow EP because the Rb(nl) would be a product of the EP reaction and it would also require another Rb in its 5p state to be present. As explained, one of the reasons the EP process is negligible is that the Rb(5p) transition rate to Rb(5s) of 10^7 Hz is much faster than the rate of 10^4 Hz of the EP reaction, therefore, the probability of a Rb(5p) being present once products of the EP are formed would be minuscule, thus, the ionization process described in equation 7 is excluded from being a potential ionization pathway.

4 Conclusion

The Rb fluorescence detected at 422 nm ($6p \rightarrow 5s$) when Rb is pumped on its D_2 transition at 780 nm was used to study the multiphoton excitation and ionization kinetics of Rb mixed with He as a buffer gas. By using the radiation trapping characteristics of the D_2 fluorescence of Rb in a buffer gas, the population densities of the metal were calculated and used in the model for the analysis of the 422 nm signal. This analysis suggests that when the Rb-He vapor is irradiated with high powers at 780nm, Rb^+ is formed by multiphoton absorption and, through a collisional process with Rb and He, it produces Rb_2^+ . Rb_2^+ then undergoes recombination with an electron to yield two Rb atoms, with one of them emitting fluorescence at 422nm. These results suggest that energy pooling processes between Rb atoms are negligible. If the 422nm fluorescence results from an ionization process, as suggested in this report, the temporary presence of ions would produce a transient current; further work would include placing electrodes in the apparatus to determine if the fluorescence observed can be correlated with the transient current in the cell. The ionization of the metal being instantaneous with the photoexcitation pulse, the model presented could also be tested by performing analogous experiments with a one photon ionization, using ultraviolet light, of the Rb vapor and verifying that similar results for the 422nm emission are obtained.

References

1. Taibjee, S. M.; Cheung, S. T.; Laube, S.; Lanigan, S. W., Controlled study of excimer and pulsed dye lasers in the treatment of psoriasis. *British Journal of Dermatology* **2005**, *153* (5), 960-966; Alhowaish, A. K.; Dietrich, N.; Onder, M.; Fritz, K., Effectiveness of a 308-nm excimer laser in treatment of vitiligo: a review. *Lasers in Medical Science* **2013**, *28* (3), 1035-1041.
2. Wang, X.; McCulley, J. P.; Bowman, W.; Cavanagh, H. D., Results of combined myopic astigmatic LASIK treatment and retreatments. *CLAO Journal* **2002**, *28* (1), 55-60.
3. Speed measuring device for ship - in which speedometer measuring circuits which measure distance of object separately by transmitting laser and ultrasonic pulse towards object and data is selected among two outputs. JP8297164-A, JP8297164-A 12 Nov 1996 G01S-015/00 199704 Pages: 4.
4. Ballato, J.; Dragic, P., Materials Development for Next Generation Optical Fiber. *Materials* **2014**, *7* (6), 4411-4430.
5. Basting, D.; Govorkov, S.; Paetzel, R.; Bragin, I.; Targsdorf, A. Excimer or molecular fluorine laser system for applications in micro-lithography and semiconductor processing, includes common pulser circuit that drives respective chambers. US2005031004-A1; US7308013-B2, US2005031004-A1 10 Feb 2005 H01S-003/22 200522 Pages: 30 US7308013-B2 11 Dec 2007 H01S-003/14 200781.
6. Krupke, W. F., Diode pumped alkali lasers (DPALs)—A review (rev1). *Progress in Quantum Electronics* **2012**, *36* (1), 4-28.
7. Rice, C. A.; Lott, G. E.; Perram, G. P., Open-path atmospheric transmission for a diode-pumped cesium laser. *Applied Optics* **2012**, *51* (34), 8102-8110.
8. Miller, W. S.; Sulham, C. V.; Holtgrave, J. C.; Perram, G. P., Limitations of an optically pumped rubidium laser imposed by atom recycle rate. *Applied Physics B-Lasers and Optics* **2011**, *103* (4), 819-824.
9. Barton, D. K.; Moncton, D.; Falcone, R.; Montague, D.; Kleppner, D.; Mosher, D. E.; Lamb, F. K.; Priedhorsky, W.; Lau, M. K.; Tigner, M.; Lynch, H. L.; Vaughan, D. R., Report of the American Physical Society Study Group on Boost-Phase Intercept Systems for National Missile Defense: Scientific and Technical Issues. *Rev Mod Phys* **2004**, *76* (3), 1-+.
10. Gao, F.; Chen, F.; Xie, J. J.; Li, D. J.; Zhang, L. M.; Yang, G. L.; Guo, J.; Guo, L. H., Review on diode-pumped alkali vapor laser. *Optik* **2013**, *124* (20), 4353-4358.
11. Wang, Y.-J.; Pan, B.-L.; Zhu, Q.; Yang, J., A kinetic model for diode pumped Rubidium vapor laser. *Optics Communications* **2011**, *284* (16-17), 4045-4048.
12. Heaven, M. C., Recent advances in the development of discharge-pumped oxygen-iodine lasers. *Laser & Photonics Reviews* **2010**, *4* (5), 671-683.
13. Quarrie, L. O. B., The effects of atomic rubidium vapor on the performance of optical windows in Diode Pumped Alkali Lasers (DPALs). *Optical Materials* **2013**, *35* (5), 843-851.
14. Readle, J. D.; Eden, J. G.; Verdeyen, J. T.; Carroll, D. L., Four level, atomic Cs laser at 852.1 nm with a quantum efficiency above 98%: Observation of three body photoassociation. *Applied Physics Letters* **2010**, *97* (2).
15. Readle, J. D. ATOMIC ALKALI LASERS PUMPED BY THE DISSOCIATION OF PHOTOEXCITED ALKALI-RARE GAS COLLISION PAIRS. University of Illinois at Urbana-Champaign, 2010.
16. Pitz, G. A.; Fox, C. D.; Perram, G. P., Pressure broadening and shift of the cesium D-2 transition by the noble gases and N-2, H-2, HD, D-2, CH4, C2H6, CF4, and He-3 with comparison to the D-1 transition. *Physical Review A* **2010**, *82* (4).

17. Barmashenko, B. D.; Rosenwaks, S.; Heaven, M. C., Static diode pumped alkali lasers: Model calculations of the effects of heating, ionization, high electronic excitation and chemical reactions. *Optics Communications* **2013**, *292*, 123-125.
18. Krupke, W. F.; Beach, R. J.; Kanz, V. K.; Payne, S. A., Resonance transition 795-nm rubidium laser. *Opt. Lett.* **2003**, *28* (23), 2336-2338.
19. Sulham, C. V.; Perram, G. P.; Wilkinson, M. P.; Hostutler, D. A., A pulsed, optically-pumped rubidium laser at high pump intensity. *Optics Communications* **2010**, *283* (21), 4328-4332.
20. Han, J. D.; Heaven, M. C., Gain and lasing of optically pumped metastable rare gas atoms. *Optics Letters* **2012**, *37* (11), 2157-2159.
21. Tam, A.; Moe, G.; Happer, W., PARTICLE FORMATION BY RESONANT LASER LIGHT IN ALKALI-METAL VAPOR. *Physical Review Letters* **1975**, *35* (24), 1630-1633.
22. Brown, K. C.; Perram, G. P., Spin-orbit relaxation and quenching of cesium 7 P-2 in mixtures of helium, methane, and ethane. *Physical Review A* **2012**, *85* (2).
23. Zhdanov, B. V.; Knize, R. J., Hydrocarbon-free potassium laser. *Electronics Letters* **2007**, *43* (19), 1024-1025.
24. Readle, J. D.; Wagner, C. J.; Verdeyen, J. T.; Spinka, T. M.; Carroll, D. L.; Eden, J. G., Excimer-pumped alkali vapor lasers: A new class of photoassociation lasers. In *High Energy/Average Power Lasers and Intense Beam Applications Iv*, Davis, S. J.; Heaven, M. C.; Schriempf, J. T., Eds. 2010; Vol. 7581.
25. Nakayama, A.; Niimi, K.; Ono, Y.; Taketsugu, T., Competing effects of rare gas atoms in matrix isolation spectroscopy: A case study of vibrational shift of BeO in Xe and Ar matrices. *J Chem Phys* **2012**, *136* (5).
26. Ryan, M.; Collier, M.; de Pujo, P.; Crepin, C.; McCaffrey, J. G., Investigations of the Optical Spectroscopy of Atomic Sodium Isolated in Solid Argon and Krypton: Experiments and Simulations. *J Phys Chem A* **2010**, *114* (9), 3011-3024.
27. Jacquet, E.; Zanuttini, D.; Douady, J.; Giglio, E.; Gervais, B., Spectroscopic properties of alkali atoms embedded in Ar matrix. *J Chem Phys* **2011**, *135* (17).
28. Arimondo, E.; Giammanco, F.; Sasso, A.; Schisano, M. I., LASER IONIZATION AND TIME-RESOLVED ION COLLECTION IN CESIUM VAPOR. *Optics Communications* **1985**, *55* (5), 329-334.
29. Cheret, M.; Barbier, L.; Lindinger, W.; Deloche, R., PENNING AND ASSOCIATIVE IONIZATION OF HIGHLY EXCITED RUBIDIUM ATOMS. *J Phys B-at Mol Opt* **1982**, *15* (19), 3463-3477.
30. Mahmoud, M. A., Kinetics of Rb-2(+) and Rb+ formation in laser-excited rubidium vapor. *Central European Journal of Physics* **2008**, *6* (3), 530-538.
31. Sulham, C. V.; Pitz, G. A.; Perram, G. P., Blue and infrared stimulated emission from alkali vapors pumped through two-photon absorption. *Applied Physics B-Lasers and Optics* **2010**, *101* (1-2), 57-63.
32. Kasalica, B.; Stojadinovic, S.; Belca, I.; Sarvan, M.; Zekovic, L.; Radic-Peric, J., The anomalous sodium doublet D-2/D-1 spectral line intensity ratio - a manifestation of CCD's presaturation effect. *Journal of Analytical Atomic Spectrometry* **2013**, *28* (1), 92-97.
33. Baig, M. A.; Mahmood, S.; Kalyar, M. A.; Rafiq, M.; Amin, N.; Haq, U., Oscillator strength measurements of the 3p -> nd Rydberg transitions of sodium. *European Physical Journal D* **2007**, *44* (1), 9-16.
34. Rotondaro, M. D.; Perram, G. P., Collisional broadening and shift of the rubidium D-1 and D-2 lines (5(2)S(1/2)->5(2)P(1/2), 5(2)P(3/2)) by rare gases, H-2, D-2, N-2, CH4 and CF4. *J Quant Spectrosc Ra* **1997**, *57* (4), 497-507.

35. Sell, J. F.; Gearba, M. A.; Patterson, B. M.; Byrne, D.; Jemo, G.; Lilly, T. C.; Meeter, R.; Knize, R. J., Collisional excitation transfer between Rb(5P) states in 50-3000 Torr of He-4. *J Phys B-at Mol Opt* **2012**, *45* (5), 10.
36. Zamoski, N. D.; Rudolph, W.; Hager, G. D.; Hostutler, D. A., A study of collisional quenching and radiation-trapping kinetics for Rb(5p) in the presence of methane and ethane using time-resolved fluorescence. *J Phys B-at Mol Opt* **2009**, *42* (24).
37. Steck, D. A., Rubidium 87 D Line Data. **2003**.
38. Theodosiou, C. E., LIFETIMES OF ALKALI-METAL - ATOM RYDBERG STATES. *Physical Review A* **1984**, *30* (6), 2881-2909.
39. Barbier, L.; Cheret, M., ENERGY POOLING PROCESS IN RUBIDIUM VAPOR. *Journal of Physics B-Atomic Molecular and Optical Physics* **1983**, *16* (17), 3213-3228.
40. Caiyan, L.; Ekers, A.; Klavins, J.; Jansons, M., Studies of inelastic cross-section in Rb(7S)+Rb(5S) collisions. *Physica Scripta* **1996**, *53* (3), 306-308.
41. Shen, Y. F.; Dai, K.; Mu, B. X.; Wang, S. Y.; Cui, X. H., Energy-pooling collisions in rubidium: $5P(3/2)+5P(3/2)\rightarrow 5S+(nl=5D, 7S)$. *Chinese Physics Letters* **2005**, *22* (11), 2805-2807.
42. Safronova, M. S.; Safronova, U. I., Critically evaluated theoretical energies, lifetimes, hyperfine constants, and multipole polarizabilities in Rb-87. *Physical Review A* **2011**, *83* (5).